

Catalysis Science & Technology

Accepted Manuscript

This article can be cited before page numbers have been issued, to do this please use: J. M. Doña-Rodríguez, R. Quesada-Cabrera, D. R. MacFarlane, A. N. Simonov and L. M. Azofra, *Catal. Sci. Technol.*, 2026, DOI: 10.1039/D6CY00192K.



This is an Accepted Manuscript, which has been through the Royal Society of Chemistry peer review process and has been accepted for publication.

Accepted Manuscripts are published online shortly after acceptance, before technical editing, formatting and proof reading. Using this free service, authors can make their results available to the community, in citable form, before we publish the edited article. We will replace this Accepted Manuscript with the edited and formatted Advance Article as soon as it is available.

You can find more information about Accepted Manuscripts in the [Information for Authors](#).

Please note that technical editing may introduce minor changes to the text and/or graphics, which may alter content. The journal's standard [Terms & Conditions](#) and the [Ethical guidelines](#) still apply. In no event shall the Royal Society of Chemistry be held responsible for any errors or omissions in this Accepted Manuscript or any consequences arising from the use of any information it contains.

COMMUNICATION

Enhanced N_2 capture and cleavage promoted by lithium nanoparticles†Received XXth XXX 20XX,
Accepted XXth XXX 20XXJosé Miguel Doña-Rodríguez,^a Raúl Quesada-Cabrera,^a Douglas R. MacFarlane,^b Alexandr N. Simonov^{*b} and Luis Miguel Azofra^{*a}

DOI: 10.1039/X0XX00000X

Activation of N_2 with metallic lithium is a key step of the lithium redox-mediated nitrogen reduction reaction (Li-NRR) – a process that can enable practical ammonia electro-synthesis under mild conditions. Our present DFT study revealed that N_2 capture and $N\equiv N$ bond cleavage is substantially enhanced on and within Li^0 nanoparticles as compared to bulk slabs. This behaviour is not limited to single-molecule adsorption but is also observed during the successive capture of additional N_2 molecules. The results presented herein might assist in the design of higher performance Li-NRR systems.

The nitrogen reduction reaction (NRR) is one of the most extensively studied processes of the last decade in the field of applied electrocatalysis, owing to the importance of ammonia as a fertiliser feedstock and a future energy vector.¹ However, research on the electrochemical N_2 activation under mild conditions has demonstrated that the direct electrocatalytic reduction of N_2 is challenging to achieve at production rates that are viable on a practical scale.² In contrast, the lithium redox-mediated NRR (Li-NRR) has been unambiguously proven to provide practical levels of genuine conversion of N_2 into NH_3 at ambient temperature and very mild pressure <20 bar.^{3–7}

In the Li-NRR, the electrochemically generated metallic lithium mediates N_2 cleavage with the formation of lithium nitride *via* a dissociative mechanism, which demonstrate a range of distinctive features^{8–10} as compared to the mechanisms of N_2 activation proposed for the direct electrocatalytic NRR.^{11–18} Next, the nitrogen atoms incorporated into the Li_3N lattice are converted into NH_3 through successive protonation by a suitable proton carrier.^{19,20} A similar mechanism has recently been reported for calcium²¹ and magnesium.²²

At a theoretical level, this behaviour has been modelled in metal slabs, in the first instance for the N_2 cleavage mechanism

(Figure 1),^{8–10} but also in subsequent protonation steps.^{23,24} These previous studies established that: (i) end-on adsorption of N_2 on Li^0 is non-spontaneous; (ii) side-on adsorption, by contrast, is spontaneous, overcoming the physisorption regime, as N_2 becomes inserted into the surface structure of the Li^0 slabs, with binding free energies characteristic of chemisorption or capture events; (iii) N_2 can diffuse into the inner layers of the Li^0 bulk; and (iv) the activation free-energy barriers for N_2 cleavage on the Li^0 surface or within the Li^0 bulk are accessible at room temperature.

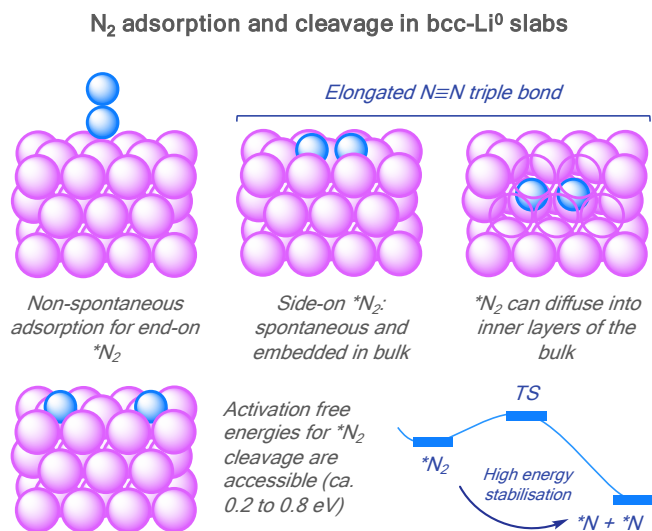


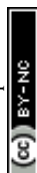
Figure 1. Summary of the main chemical events observed during the N_2 capture and cleavage on and within the bcc- Li^0 slabs.^{8,9}

However, metal slabs represent restricted structures, in contrast to nanoparticles which exhibit diverse structural features, like different facets as well as edges and corners. These features are likely relevant to the real state of the electroplated Li^0 intermediate during the Li-NRR, since electrodeposition of lithium metal typically produces highly heterogeneous nanostructured aggregates rather than well-defined crystalline surfaces.^{25–27} To investigate this, we conducted a density functional theory (DFT) study

^a Instituto de Estudios Ambientales y Recursos Naturales (i-UNAT), Universidad de Las Palmas de Gran Canaria (ULPGC), Campus de Tafira, 35017 Las Palmas de Gran Canaria, Spain. E-mail: luismiguel.azofra@ulpgc.es

^b School of Chemistry, Monash University, Clayton, Victoria 3800, Australia. E-mail: alexandr.simonov@monash.edu

† Supplementary Information available: methodological aspects, full computational details. See DOI:10.1039/X0XX00000X



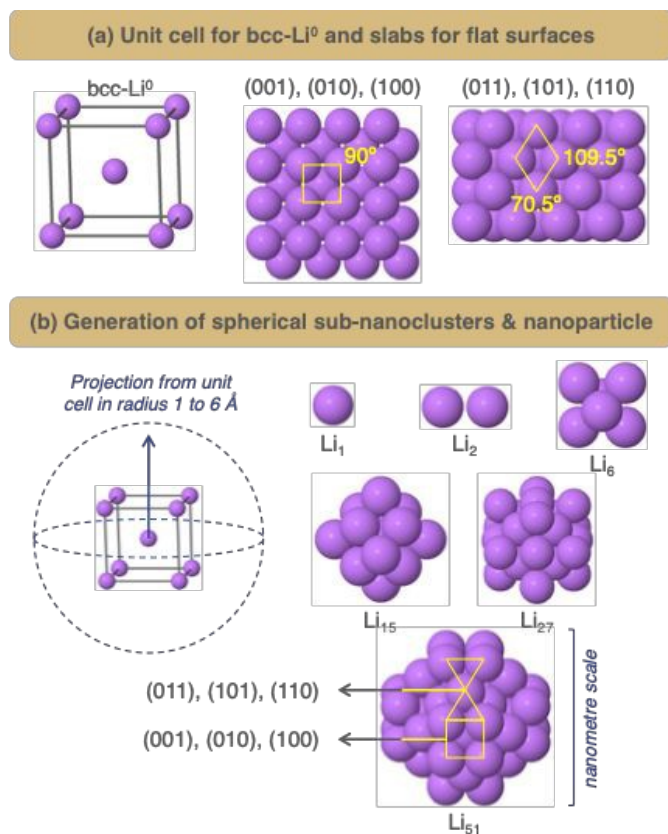


Figure 2. (a) Most common flat surfaces (top view) of bcc-Li⁰: (001), equivalent to (010) and (100), and (011), equivalent to (101) and (110). (b) Generation of sub-nanoclusters and nanoparticle models *via* spherical projection of the bcc-Li⁰ unit cell, resulting in Li₁ (radius, $r = 1$ Å), Li₂ ($r = 2$ Å), Li₆ ($r = 3$ Å), Li₁₅ ($r = 4$ Å), Li₂₇ ($r = 5$ Å), and Li₅₁ ($r = 6$ Å).

(pseudopotential plane-wave method, RPBE²⁸+D3^{29,30} level of theory, VASP,^{31–34} see Supplementary Information, SI, for computational details) of a series of structures that were modelled by spherically projecting the body-centred cubic (bcc) Li⁰ unit cell with radii ranging from 1 to 6 Å. This resulted in a series of initial models: the Li₁ atomic dot (1 Å radius), the Li₂ (2 Å), Li₆ (3 Å), Li₁₅ (4 Å) and Li₂₇ (5 Å) sub-nanoclusters, and the Li₅₁ (6 Å) nanoparticle (**Figure 2**).

In our previous study on the interaction of N₂ on and within the bcc-Li⁰ slabs, we computed binding free energies for the (001) and (011) flat surfaces, amongst others.^{8,9} We found that end-on N₂ adsorption exhibited non-spontaneous values of 0.22 eV in both cases, whereas side-on adsorption was spontaneous, with values of –0.46 and –0.66 eV, respectively. The computational protocol used in that study differs from the one employed herein in the calculation of vibrational frequencies only, where atomic positions of the metal were frozen in the previously published work.^{8,9} While slabs can be considered constrained structures due to their periodicity, this assumption does not hold for nanostructures. Consequently, when recalculating the side-on N₂ binding on the (001) and (011) facets without structural constraints in the frequency calculation, the values changed slightly to –0.35 and –0.55 eV,

respectively. By applying a consistent methodology, comparison of the N₂-adsorption results computed here for our sub-nanoclusters and nanoparticle models with those for metal slabs was therefore straightforward.

Interestingly, both Li₁ and Li₂ – the simplest models examined herein – exhibited highly non-spontaneous N₂ binding free energies (ΔG_b). For instance, the linear end-on minima (labelled [1] in both cases in **Figure 3**) showed ΔG_b values of 0.36 and 0.34 eV, respectively, along with minimal N≡N bond elongations of 0.03 and 0.01 Å, compared with the nitrogen–nitrogen distance of 1.12 Å for N₂(g) obtained using this computational protocol. These energy values were similar or even less favourable than those of other structures considered herein, specifically minimum [2] for Li₁ of side-on type (0.54 eV), and minima [2] and [3] for Li₂ of angular end-on (0.31 eV) and side-on (0.55 eV) types.

In principle, these results qualitatively follow the trends established before for the Li⁰ slabs, where the side-on adsorption was energetically more favourable than end-on.^{8,9} However, it was somewhat surprising to find that the interactions between N₂ and these Li⁰ structures were so endergonic, given that both Li₁ and Li₂ represent single-site models. Indeed, single-site models have demonstrated superior substrate-interaction capabilities for many other systems. For example, this was shown for the end-on interaction of N₂ with iron slabs³⁵ and with a single iron atom,³⁶ where the binding energy in the latter case is increased by nearly a factor of seven, although we acknowledge that, in this model, the single-site iron atom was not isolated but supported on a MoS₂ sheet. However, in the case of Li⁰, energetically favourable N₂–metal interactions seem to demonstrate an opposite trend.

Li₆ formally represents a cluster-type structure of a square-based bipyramid. In this case, we observe binding events that deviate from the general trend in N₂-philicity exhibited by Li⁰ slabs. Four minima were identified for this model: the linear end-on minimum, labelled [1], was slightly physisorbed with a spontaneous ΔG_b (*ca.* –0.1 eV), whereas ΔG_b values were endergonic for minima [2]–[4], despite [2] and [3] being side-on (the former interacting with three Li centres and the latter with two) (**Figure 3**).

Note that two binding free energy values are reported for all lithium models, except Li₁ and Li₂, considered herein because, unlike metallic slabs, they undergo distortions relative to their original structures. The first ΔG_b value refers to the free energy difference between the minimum in question and the perfectly symmetric cluster. The second ΔG_b was calculated by re-optimising the cluster structure after removal of the adsorbed N₂ molecule. The difference between the two values provides a measure of the energy associated with cluster structure deformation. It should be noted that the deformation energy discussed herein does not necessarily reflect the stability of Li⁰ nanostructures during Li-NRR. A proper assessment of this aspect would require a separate investigation involving additional species participating in the reaction.

For the Li₆ cluster, this difference was negligible, meaning almost no deformation with respect to the perfectly symmetrical cluster of this type (**Figure 3**). In contrast, the



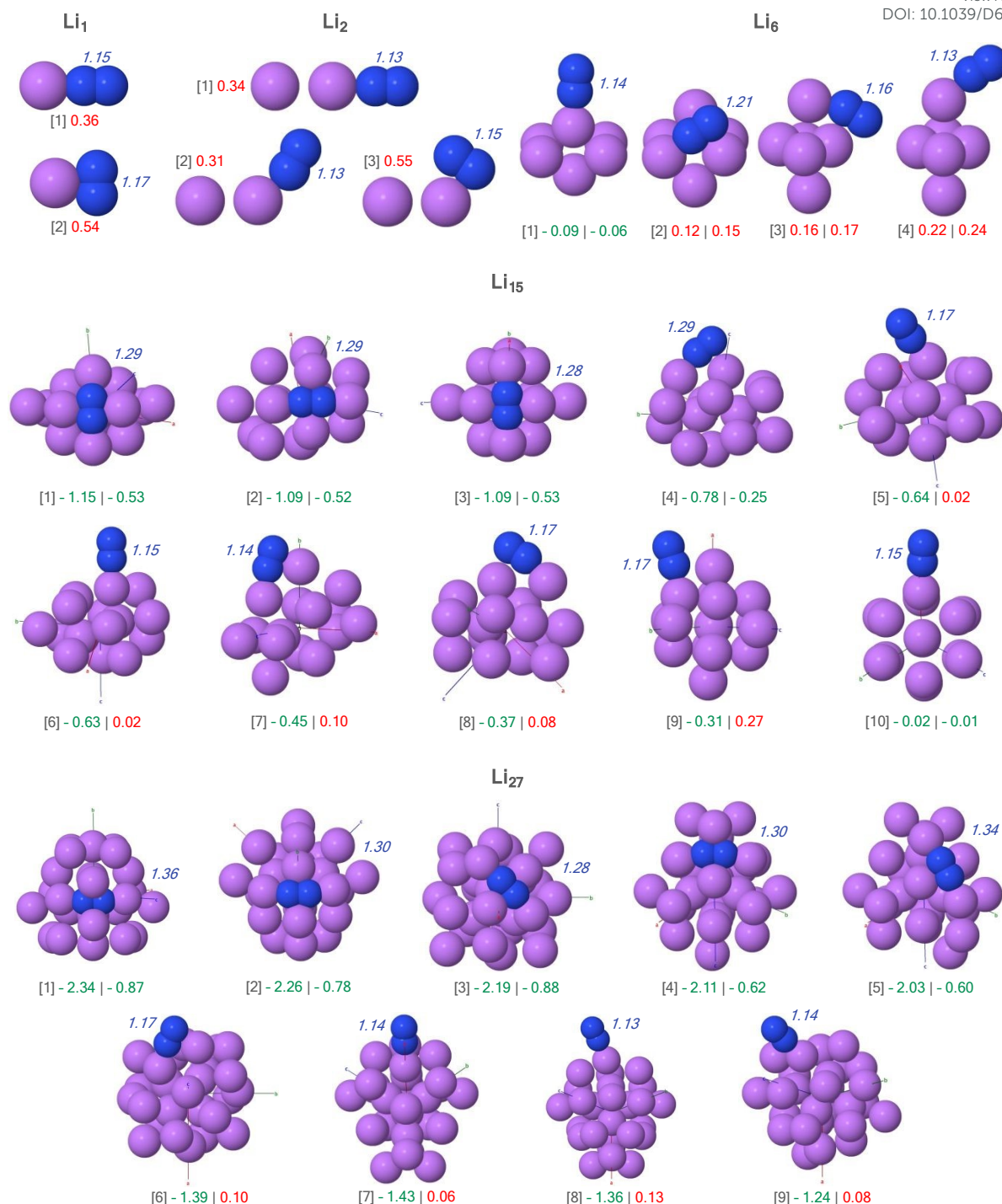


Figure 3. *N₂ minima obtained for the Li₁ atomic dot and the Li₂, Li₆, Li₁₅, and Li₂₇ sub-nanoclusters. N≡N distances (in Å) are shown in *blue*. Binding free energies (in eV) are indicated in green for spontaneous and red for non-spontaneous values. For the Li₁₅ and Li₂₇ models, Cartesian axes (a, b, c, corresponding to OX, OY, and OZ, respectively) are also shown as a reference for orientation, facilitating comparison with the symmetric structures presented in **Figure 2**.

change was particularly pronounced for the Li₁₅ model, where the cluster deformation energies were, in most cases, around -0.6 eV; that is, the distorted structures were more stable than the initial perfectly symmetric cluster. From the perspective of formal analysis of N₂ stabilisation, it is the second ΔG_b value that is of major interest.

For Li₁₅, the binding free energies of N₂ were similar to those computed for the slabs, with values of -0.53, -0.52, and -0.53 eV for the first three minima, which: (i) are of side-on type; (ii) correspond to molecules embedded within the cluster surface; and (iii) show that superficial interactions lead to the decreased ΔG_b values (**Figure 3**). We also observed that the



captured N_2 molecules in these more stable configurations were activated, with elongated $N\equiv N$ bonds to approximately 1.3 Å. Although the ΔG_b values for these three most stable minima were similar, their electronic energies, *i.e.*, not including enthalpic and entropy contributions, differed by more than 0.1 eV (≈ 9.65 kJ mol $^{-1}$), confirming that they represent distinct structures on the potential energy surface (PES).

The binding free energy results for the Li_{27} model further emphasised the intensification of the N_2-Li^0 interactions within atom clusters as compared to the slab models. We identified a series of side-on and embedded N_2 minima, labelled [1]–[5], whereas minima [6]–[9] correspond to mixed ([6]), angular ([7]), and linear end-on ([8]–[9]) types (Figure 3). For the former (side-on), ΔG_b was exergonic, while for the latter (mixed and end-on) it was not. This behaviour, although somewhat expected, would not be particularly noteworthy if the N_2 binding free energy values did not significantly exceed the reference values obtained for slabs (–0.55 eV). In these clusters, the interactions reached as much as –0.9 eV, indicating that N_2 capture was strongly enhanced, accompanied by substantial activation of the molecule. For instance, for side-on minima [1]–[5], $N\equiv N$ bond lengths ($r_{N\equiv N}$) elongated up to 1.28–1.36 Å (Figure 3).

To explore if this improved N_2 fixation could be maintained, and to what extent, at the nano- rather than sub-nanometre

scale discussed above, we further studied the Li_{51} nanoparticle model. The intensity of N_2 capture in Li_{51} followed a pattern similar to that observed in the Li_{27} cluster: side-on and embedded N_2 structures on the nanoparticle surface exhibited ΔG_b values ranging from –0.88 eV for the most stable to –0.60 eV for the least stable, whereas end-on interactions remained endergonic. This is exemplified in Figure 4a for the three most stable N_2 minima identified for the Li_{51} model, with the remaining minima provided in Figures S2. Notably, the $N\equiv N$ bond elongation was slightly greater than that observed for the corresponding minima in the Li_{27} model, and distortion energies were somewhat higher, indicative of enhanced stability in the non-symmetric Li_{51} nanoparticle compared with the symmetric structure (*cf.* data in Figure 3 and Figure 4a). A correlation between ΔG_b and the number of lithium atoms interacting with N_2 was noted for $*N_2$ minima in both the Li_{27} and Li_{51} models (Figure S5), consistent with our observation that binding free energy became stronger as the number of the $Li\cdots N$ bonds increased.

In light of these results obtained for the larger nanostructures, Li^0 appears to exhibit a pronounced affinity towards N_2 . Nevertheless, further investigations including explicit solvent molecules will be required to evaluate possible competitive adsorption effects under more realistic conditions.

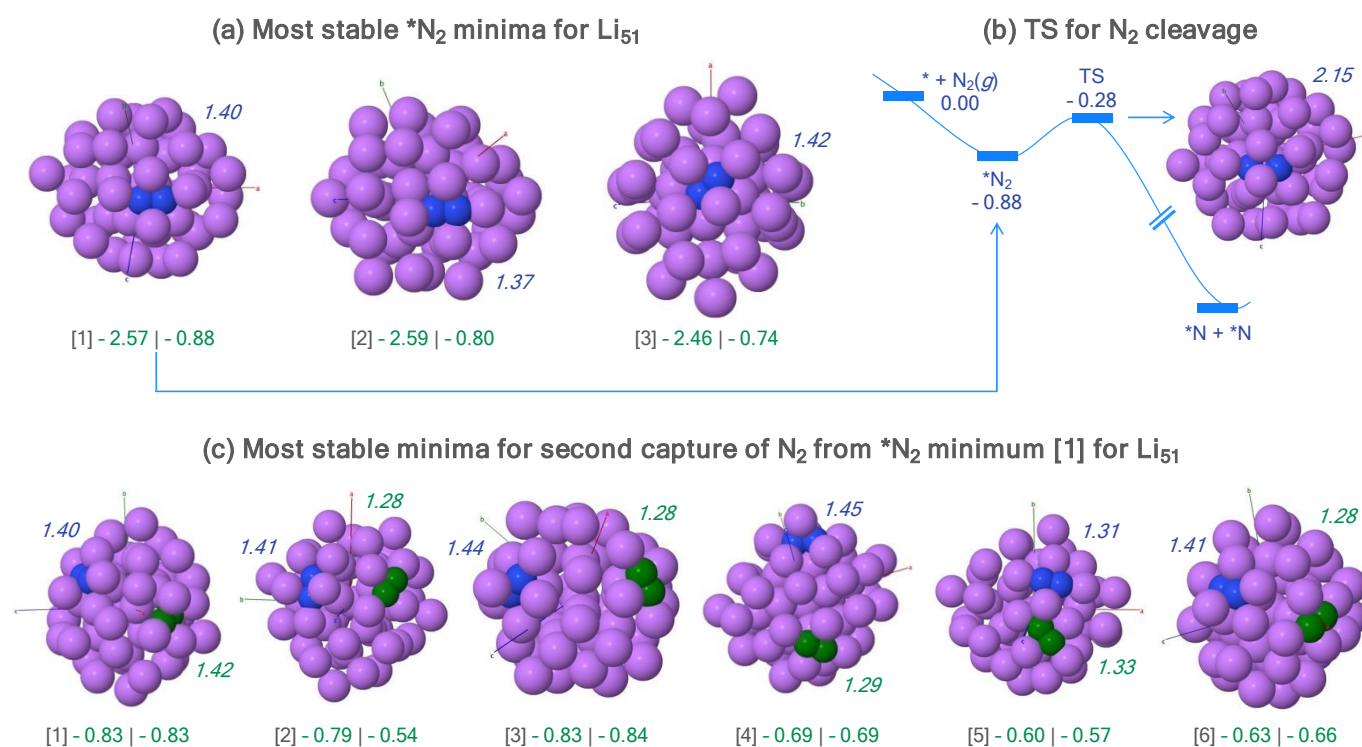


Figure 4. (a) Most stable $*N_2$ minima (all side-on) obtained for the Li_{51} nanoparticle. (b) Potential energy surface (PES) for N_2 capture and cleavage of minimum [1] in the Li_{51} model, including the optimised structure of the $N\equiv N$ cleavage transition state. (c) Most stable minima for a second N_2 capture, where the original $*N_2$ from minimum [1] is shown in blue and the second $*N_2$ in green. $N\equiv N$ distances (in Å) are shown in *italics*, following the same colour code.



Further, we sought to explore fundamental aspects of the N_2 cleavage mediated by the lithium metal nanoparticle by addressing two questions: (i) what is the energy cost (activation barrier) associated with cleaving the $*N_2$ molecule into N adatoms ($*N$) during the formation of lithium nitride; and (ii) is capture of a second N_2 molecule also an energetically favourable process?

Addressing the first question, the computed activation energies for the lithium-mediated dinitrogen dissociation process were low to moderate, that is, with values less than 1 eV. Specifically, we performed calculations to locate the transition states (TSs) for N_2 cleavage of the six most stable side-on N_2 minima in the Li_{51} model, obtaining values ranging from 0.46 eV for the lowest barrier to 0.64 eV for the highest (Table S3 and Figure S3). Remarkably, all activation barriers were smaller, in absolute terms, than the energy released upon N_2 chemisorption. This is exemplified in Figure 4b for the minimum [1] of the Li_{51} model. In this case, the $* + N_2(g) \rightarrow *N_2$ physical process exhibited a free energy drop of -0.88 eV, as discussed previously, and an activation barrier of 0.61 eV relative to this state. Additionally, the chemisorbed N_2 molecule showed a bond elongation of 0.28 Å ($r_{N=N} = 1.40$ Å), while the nitrogen–nitrogen distance in the TS was 2.15 Å.

To assess the kinetic accessibility of the embedded N_2 -in- Li^0 configurations, a constrained approach scan was performed for the Li_{51} model in which the central Li atom and N_2 distance was progressively reduced while relaxing the remaining degrees of freedom (see Figure S6). The resulting profile reveals a very small electronic energy barrier of 0.14 eV for N_2 penetration into the subsurface region, followed by stabilisation of the embedded state. This indicates that subsurface incorporation is kinetically accessible within the capabilities of the static DFT approach employed herein.

To explore the capability of a lithium nanoparticle to activate multiple dinitrogen molecules, a second N_2 was randomly placed at various positions onto the $*N_2$ minimum [1] of the Li_{51} model. The capture of an additional N_2 molecule was found to be spontaneous, with structural distortion energies being practically negligible. In more detail, Figure 4c shows six of the nineteen minima identified for this case, while the remaining structures are provided in Figure S4. Notably, for all these minima, the second N_2 molecule adopted a side-on configuration in the most stable structures (shown in green in Figure 4c), with spontaneous ΔG_b values generally comparable to those computed for the first captured N_2 molecule (blue in Figure 4c). Although the $N=N$ bond in the second N_2 molecule was also elongated, the magnitude of this effect was less pronounced. By contrast, for all these minima, the bond elongation of the first captured N_2 molecule was maintained or even enhanced, with $N=N$ distances exceeding 1.4 Å in some cases (Figure S4).

Based on these results, Li^0 nanoparticles can be considered exceptionally effective N_2 capturers, even more effective than the slab models. To further support this conclusion, we performed NVT [substance (N), volume (V), temperature (T); canonical ensemble] molecular dynamics (MD) simulations starting from an initial configuration in which thirty-six N_2

molecules were positioned in an end-on orientation, pointing towards each of the surface lithium atoms of the Li_{51} nanoparticle and placed at a distance of 3 Å. This setup established unfavourable initial conditions, namely, N_2 molecules at distances corresponding to non-adsorptive interactions and in an end-on orientation, which, as confirmed by our calculations, were non-spontaneous. If the Li_{51} nanoparticle indeed behaves as a highly potent N_2 capturer, the MD simulation could be expected to evolve towards spontaneous adsorption and activation.

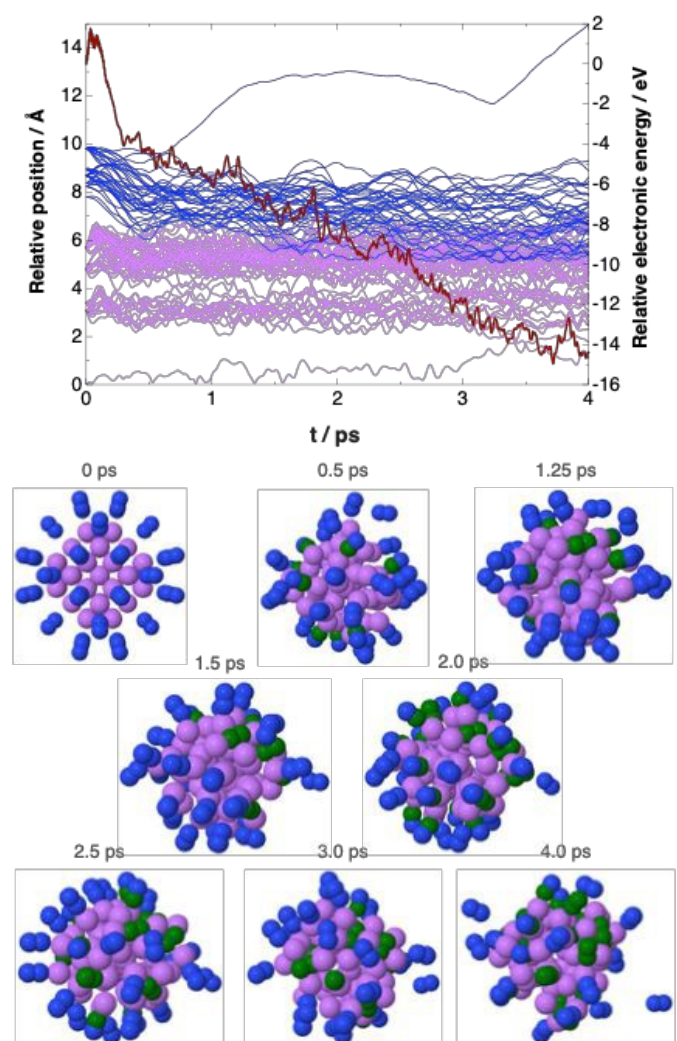


Figure 5. NVT molecular dynamics for the Li_{51} nanoparticle model surrounded by thirty-six N_2 molecules, each initially placed 3 Å away from the closest N atom interacting with Li. Relative positions (in Å) correspond to the distance of each Li atom (purple) and the centre of mass of each N_2 molecule (blue) relative to the nanoparticle's centre of mass. Evolution of electronic energy (dark red, in eV) is also shown, together with selected snapshots along the NVT MD trajectory. In these structures, N atoms of the N_2 molecules that are closer to the nanoparticle's centre of mass than the outermost Li^0 atom are highlighted in green.



The results in this regard were highly instructive. On the picosecond timescale, a progressive insertion of numerous N₂ molecules onto and within the nanoparticle was observed (Figure 5). As the MD simulation progressed, convergence of the centres of mass of the N₂ molecules with those of the Li⁰ atoms was found, indicating the point of interaction between dinitrogen and the lithium nanoparticle surface. Specifically, a substantial number of N₂ molecules were captured within inner layers of Li₅₁ after approximately 1.5 ps of the total 4 ps simulation. Throughout this evolution, up to nearly 4 ps, N₂ capture by the Li⁰ nanoparticle was accompanied by a decrease in the electronic energy (shown in dark red in Figure 5), indicating that these adsorption events were energetically stabilising. Figure 5 also includes selected snapshots along the MD trajectory, visually illustrating the progressive N₂ capture behaviour of the lithium nanoparticle.

The finding discussed above provide new insights into the chemistry governing the first critical step of the Li-NRR, viz. activation of dinitrogen. In the future, it will be important to investigate how the cleavage of a sufficiently large number of captured N₂ molecules ultimately leads to nitridation of the Li⁰ nanoparticles. Simultaneous capture of multiple N₂ molecules by the Li⁰ nanoparticles may introduce electronic interactions between adsorbates, which could influence the activation of subsequent N₂ molecules. Of an even higher interest is the location of the nitride formation, viz. at the surface or in the bulk of the particles, which might result in very different scenarios. Indeed, formation of a lithium nitride surface layer may potentially passivate Li⁰ and suppress subsequent N₂ capture. On the contrary, formation of the lithium nitride in the bulk, which might be possible owing to the N₂ diffusion through Li⁰ demonstrated herein and previously,^{8–10} might allow for the most effective utilisation of the electrochemically generated lithium metal. A detailed assessment of these effects would require a more extensive exploration of the system and is left for future investigation.

Conclusions

In summary, our DFT investigation demonstrated that Li⁰ subnanoclusters and especially nanoparticles exhibit a remarkable capability for N₂ capture and activation, surpassing that of the previously studied metal slabs. Our calculations revealed that side-on and embedded adsorption configurations are highly stabilising, with significant elongation of the N≡N bond and accessible activation barriers for cleavage, and that multiple N₂ molecules can be captured successively. Furthermore, NVT molecular dynamics simulations indicate that the highly energetically favourable capture events take place on a picosecond scale, with N₂ molecules progressively inserted into the nanoparticle's inner layers and accompanied by energy stabilisation. These findings highlight the unique mechanistic role of Li⁰ nanostructures in the lithium redox-mediated nitrogen reduction reaction and suggest that such nanoparticles may serve as highly efficient platforms for further ammonia synthesis under mild electrochemical conditions. Overall, this study provides fundamental insights into the interplay between

size, structure, and reactivity against N₂ of lithium metal, opening new avenues for the design of advanced Li-NRR catalysts.

Conflicts of interest

J.M.D.-R., R.Q.-C., and L.M.A. declare no conflicts of interest. D.R.M. and A.N.S. declare competing financial interests since they are shareholders in Jupiter Ionics Pty Ltd, a start-up company focused on commercialising ammonia production technology.

Acknowledgements

J.M.D.-R., R.Q.-C., and L.M.A. are grateful to MCIN/AEI and NextGenerationEU/PRTR for the financial support through project ref. PID2022-143294OB-I00. D.R.M. and A.N.S. acknowledge the financial support from the Australian Research Council (DP250102783). L.M.A. is a Ramón y Cajal fellow (ref RYC2021-030994-I). Gratitude is also due to the KAUST Supercomputer Laboratory (KSL), KSA, for providing the computational resources (Shaheen III). This paper is dedicated to Prof Steve Scheiner (Utah State University) in recognition of his outstanding contributions to the study of non-covalent interactions.

Notes and references

- 1 D. R. MacFarlane, P. V Cherepanov, J. Choi, B. H. R. Suryanto, R. Y. Hodgetts, J. M. Bakker, F. M. Ferrero Vallana and A. N. Simonov, *Joule*, 2020, **4**, 1186–1205.
- 2 H. Zhang, Z. Lu and Z. Wen, *Nat. Rev. Chem.*, 2025, **9**, 285–286.
- 3 J. M. McEnaney, A. R. Singh, J. A. Schwalbe, J. Kibsgaard, J. C. Lin, M. Cargnello, T. F. Jaramillo and J. K. Nørskov, *Energy Environ. Sci.*, 2017, **10**, 1621–1630.
- 4 S. Z. Andersen, M. J. Statt, V. J. Bukas, S. G. Shapel, J. B. Pedersen, K. Kreml, M. Saccoccio, D. Chakraborty, J. Kibsgaard, P. C. K. Vesborg, J. Nørskov and I. Chorkendorff, *Energy Environ. Sci.*, 2020, **13**, 4291–4300.
- 5 K. Li, S. Z. Andersen, M. J. Statt, M. Saccoccio, V. J. Bukas, K. Kreml, R. Sažinas, J. B. Pedersen, V. Shadravan, Y. Zhou, D. Chakraborty, J. Kibsgaard, P. C. K. Vesborg, J. K. Nørskov and I. Chorkendorff, *Science*, 2021, **374**, 1593–1597.
- 6 B. H. R. Suryanto, K. Matuszek, J. Choi, R. Y. Hodgetts, H.-L. Du, J. M. Bakker, C. S. M. Kang, P. V Cherepanov, A. N. Simonov and D. R. MacFarlane, *Science*, 2021, **372**, 1187–1191.
- 7 H.-L. Du, M. Chatti, R. Y. Hodgetts, P. V Cherepanov, C. K. Nguyen, K. Matuszek, D. R. MacFarlane and A. N. Simonov, *Nature*, 2022, **609**, 722–727.
- 8 D. R. MacFarlane, A. N. Simonov, T. M. Vu, S. Johnston and L. M. Azofra, *Faraday Discuss.*, 2023, **243**, 557–570.
- 9 L. M. Azofra, J. M. Doña-Rodríguez, D. R. MacFarlane and A. N. Simonov, *J. Phys. Chem. C*, 2025, **129**, 1198–1205.
- 10 T. Ludwig, A. R. Singh and J. K. Nørskov, *J. Phys. Chem. C*, 2020, **124**, 26368–26378.
- 11 Y. Abghoui, A. L. Garden, J. G. Howalt, T. Vegge and E. Skúlason, *ACS Catal.*, 2016, **6**, 635–646.



- 12 D. Wang, L. M. Azofra, M. Harb, L. Cavallo, X. Zhang, B. H. R. Suryanto and D. R. MacFarlane, *ChemSusChem*, 2018, **11**, 3416–3422.
- 13 B. H. R. Suryanto, D. Wang, L. M. Azofra, M. Harb, L. Cavallo, R. Jalili, D. R. G. Mitchell, M. Chatti and D. R. MacFarlane, *ACS Energy Lett.*, 2019, **4**, 430–435.
- 14 S. Kamiguchi, K. Asakura, T. Shibayama, T. Yokaichiya, T. Ikeda, A. Nakayama, K. Shimizu and Z. Hou, *Chem. Sci.*, 2024, **15**, 2914–2922.
- 15 Y. Jiang, Z. Chen, T. Peng, L. Jiao, X. Pan, H.-L. Jiang and X. Bao, *Angew. Chem. Int. Ed.*, 2025, **64**, e202501190.
- 16 S. C. Jesudass, S. Surendran, J. Y. Kim, T.-Y. An, G. Janani, T.-H. Kim, J. K. Kim and U. Sim, *Electrochem. Energy Rev.*, 2023, **6**, 27.
- 17 W.-Q. Li, M. Xu, J.-S. Chen and T.-N. Ye, *Adv. Mater.*, 2024, **36**, 2408434.
- 18 T. Žibert, B. Likozar and M. Huš, *ChemSusChem*, 2024, **17**, e202301730.
- 19 X. Fu, A. Xu, J. B. Pedersen, S. Li, R. Sažinas, Y. Zhou, S. Z. Andersen, M. Saccoccio, N. H. Deissler, J. B. V. Mygind, J. Kibsgaard, P. C. K. Vesborg, J. K. Nørskov and I. Chorkendorff, *Nat. Commun.*, 2024, **15**, 2417.
- 20 H.-L. Du, K. Matuszek, R. Y. Hodgetts, K. Ngoc Dinh, P. V Cherepanov, J. M. Bakker, D. R. MacFarlane and A. N. Simonov, *Energy Environ. Sci.*, 2023, **16**, 1082–1090.
- 21 X. Fu, V. A. Niemann, Y. Zhou, S. Li, K. Zhang, J. B. Pedersen, M. Saccoccio, S. Z. Andersen, K. Enemark-Rasmussen, P. Benedek, A. Xu, N. H. Deissler, J. B. V. Mygind, A. C. Nielander, J. Kibsgaard, P. C. K. Vesborg, J. K. Nørskov, T. F. Jaramillo and I. Chorkendorff, *Nat. Mater.*, 2024, **23**, 101–107.
- 22 M. Krebsz, R. Y. Hodgetts, S. Johnston, C. K. Nguyen, Y. Hora, D. R. MacFarlane and A. N. Simonov, *Energy Environ. Sci.*, 2024, **17**, 4481–4487.
- 23 V. Azumah, L. Kavalsky and V. Viswanathan, *J. Phys. Chem. C*, 2025, **129**, 2488–2501.
- 24 V. Azumah, L. Kavalsky and V. Viswanathan, *J. Catal.*, 2025, **450**, 116250.
- 25 K. N. Wood, M. Noked and N. P. Dasgupta, *ACS Energy Lett.*, 2017, **2**, 664–672.
- 26 K. B. Hatzell, X. C. Chen, C. L. Cobb, N. P. Dasgupta, M. B. Dixit, L. E. Marbella, M. T. McDowell, P. P. Mukherjee, A. Verma, V. Viswanathan, A. S. Westover and W. G. Zeier, *ACS Energy Lett.*, 2020, **5**, 922–934.
- 27 K. Dong, Y. Xu, J. Tan, M. Osenberg, F. Sun, Z. Kochovski, D. T. Pham, S. Mei, A. Hilger, E. Ryan, Y. Lu, J. Banhart and I. Manke, *ACS Energy Lett.*, 2021, **6**, 1719–1728.
- 28 B. Hammer, L. B. Hansen and J. K. Nørskov, *Phys. Rev. B*, 1999, **59**, 7413–7421.
- 29 S. Grimme, J. Antony, S. Ehrlich and H. Krieg, *J. Chem. Phys.*, 2010, **132**, 154104.
- 30 S. Grimme, S. Ehrlich and L. Goerigk, *J. Comput. Chem.*, 2011, **32**, 1456–1465.
- 31 G. Kresse and J. Hafner, *Phys. Rev. B*, 1993, **47**, 558–561.
- 32 G. Kresse and J. Hafner, *Phys. Rev. B*, 1994, **49**, 14251–14269.
- 33 G. Kresse and J. Furthmüller, *Phys. Rev. B*, 1996, **54**, 11169–11186.
- 34 G. Kresse and J. Furthmüller, *Comput. Mater. Sci.*, 1996, **6**, 15–50.
- 35 B. H. R. Suryanto, C. S. M. Kang, D. Wang, C. Xiao, F. Zhou, J. M. Azofra, L. Cavallo, X. Zhang and D. R. MacFarlane, *ACS Energy Lett.*, 2018, **3**, 1219–1224.
- 36 L. M. Azofra, C. Sun, L. Cavallo and D. R. MacFarlane, *Chem. Eue. J.*, 2017, **23**, 8275–8279.



Data Availability Statement

The material presented herein does not possess any characteristics that require additional guidance regarding its Findable, Accessible, Interoperable, and Reusable (FAIR) aspects. All supplementary materials have been prepared following best practices to ensure reproducibility, providing detailed instructions for any reader to replicate the results, subject to the necessary permissions to use the software employed in this study. Furthermore, upon publication of this article, a preprint version of its content will be deposited in my university's institutional repository, in accordance with standard institutional practice.

Dr Luis Miguel Azofra

